Eur. Phys. J. A **1**, 151–169 (1998)

THE EUROPEAN PHYSICAL JOURNAL A

Modelling the many-body dynamics of heavy ion collisions: Present status and future perspective

Ch. Hartnack[1], Rajeev K. Puri[1], J. Aichelin[1], J. Konopka[2], S.A. Bass[2], H. Stöcker[2], W. Greiner[2]

[1] Laboratoire de physique subatomique et des Technologies associées (SUBATECH), UMR Université de Nantes, CNRS, Ecole des Mines, 4 rue A. Kastler, F-44070 Nantes, France

[2] Institut für Theoretische Physik, Johann Wolfgang Goethe-Universität, Postfach 11 19 32, D-60054 Frankfurt am Main, Germany

Received: 27 November 1996 / Revised version: 14 April 1997

Communicated by V. Metag

Abstract. Basic problems of the semiclassical microscopic modelling of strongly interacting systems are discussed within the framework of Quantum Molecular Dynamics (QMD). This model allows to study the influence of several types of nucleonic interactions on a large variety of observables and phenomena occurring in heavy ion collisions at relativistic energies. It is shown that the same predictions can be obtained with several – numerically completely different and independently written – programs as far as the same model parameters are employed and the same basic approximations are made. Many observables are robust against variations of the details of the model assumptions used. Some of the physical results, however, depend also on rather technical parameters like the preparation of the initial configuration in phase space. This crucial problem is connected with the description of the ground state of single nuclei, which differs among the various approaches. An outlook to an improved molecular dynamics scheme for heavy ion collisions is given.

PACS. 25.75-q Relativistic heavy-ion collisions

I Introduction

One of the main interests of the study of relativistic heavy ion collisions is the investigation of the properties of nuclear matter at extreme densities and excitation energies. [1–8]. These investigations include the production of secondary particles, the properties of particles in a (dense) nuclear medium, the compression and repulsion of dense nuclear matter, its equilibration during the reaction and its decay into fragments and single particles. On a macroscopic level the total energy of a dense nuclear system and its decomposition into thermal and compressional parts is related to the concept of the nuclear equation of state. Since a consistent derivation of the nuclear equation of state, e.g. the energy per nucleon as a function of density and temperature, is only possible in the low density limit (Brückner theory) a reliable theoretical description is not at hand. On the other hand this quantity is of interest for many astrophysical questions [14] and therefore its knowledge is highly desirable. Heavy ion reactions in combination with corresponding simulations using a variety of parametrizations of the equation of state are presently the only possible approach to study this quantity.

Heavy ion collisions allow to search for a large number of observables which may be used as indicators of the properties of matter under extreme conditions. Frequently these observables are related to the quantitative description of collective effects like the bounce–off of cold spectator matter in the reaction plane [9] and the squeeze–out of hot and compressed participant matter perpendicular to the reaction plane [10] as well as to the production of secondary particles [11–13].

Experiments performed at LBL in the early 80's (Streamer chamber, Plastic ball) yield first 4π information of the final momentum distributions in heavy ion reactions [15,16]. New experimental 4π setups at LBL, Ganil, GSI and Brookhaven enable precise measurements on the emission of primary and secondary particles and therefore provide a stimulating challenge to the theoretical description of heavy ion collisions.

Lots of comparisons have been made between experimental data and microscopic and macroscopic transport-theoretical calculations. Besides other microscopic models like VUU [17], BUU [18,19], Landau-Vlasov [20], AMD [22] or FMD [21] the Quantum Molecular Dynamics approach (QMD) is a frequently used model [23]. However, from recent comparisons of experimental results with QMD using different numerical realizations conflicting results have been reported [24]. We will demonstrate that these discrepancies are on the one hand due to the variation of physical parameters (like ground state densities, interaction ranges) whose precise values are not known. On the other hand they are a consequence of the impossi-

bility to build a ground state nucleus with all its detailed structure in a semiclassical molecular approach.

This paper is organized as follows: First the basic principles of a microscopic modelling of heavy ion reactions are briefly reported. The assumptions entering in the different QMD realizations are described in detail. The origin of differences is critically examined in this context. We demonstrate that most of the discrepancies can be attributed to different descriptions of the initial nuclei, which limits the applicability of some versions. Finally an outlook to a new molecular dynamics scheme for heavy ion collisions simulations is given.

II Microscopic modelling of heavy ion reactions

Presently the microscopic models can be subdivided into two classes: Those which follow the time evolution of the one-body phase space distribution and those which are based on n-body molecular dynamics or cascade schemes.

A VUU-type models

The microscopic transport models for the one-body Wigner phase space density distribution obtained different names although they solve the same equation. They differ in the technical realization, i.e. the computer program, and are known as Vlasov–Uehling–Uhlenbeck (VUU) model [17, 27] (or BUU [18,19], LV [20]). They solve the following transport equation for the one-body Wigner density $f(\boldsymbol{r},\boldsymbol{p},t)$ in the limit $\hbar \to 0$:

$$\begin{aligned}\frac{\partial f}{\partial t} + \boldsymbol{v}\cdot\nabla_r f - \nabla_r U\cdot\nabla_p f \quad &= \quad -\frac{4\pi^3(\hbar c)^4}{\hbar(mc^2)^2} \\ &\times \int \frac{\mathrm{d}^3p_1'}{(2\pi\hbar)^3}\,\frac{\mathrm{d}^3p_2'}{(2\pi\hbar)^3}\,\mathrm{d}^3p_2\,\frac{\mathrm{d}\sigma}{\mathrm{d}\Omega} \\ &\times [f f_2(1-f_1')(1-f_2') - f_1' f_2'(1-f)(1-f_2)] \\ &\times \delta^4(p+p_2-p_1'-p_2'). \end{aligned} \tag{1}$$

The l.h.s. of this equation is the total differential of f with respect to the time assuming a momentum independent potential U. This potential is calculated selfconsistently and corresponds to the real part of the Brückner G-matrix. Usually a Skyrme-parametrization

$$U = \alpha\left(\frac{\rho}{\rho_0}\right) + \beta\left(\frac{\rho}{\rho_0}\right)^{\gamma} \tag{2}$$

of the real part of the G-matrix is employed, where ρ is the nuclear density which is frequently measured in units of the saturation density ρ_0 of cold nuclear matter.

The r.h.s. of (1) contains a Boltzmann collision integral, which is identified with the imaginary part of the G-matrix. This part describes the influence of binary hard-core collisions, where the term with ff_2 describes the loss of particles (in a phase space region) and the term with $f_1'f_2'$ the gain term due to collisions feeding the considered phase space region. It is supplemented with the Nordheim–Uehling–Uhlenbeck modifications in order to obey the Pauli-principle in the final state of the collisions [28]. The δ-functions assure the conservation of the four-momentum. The cross section σ is normally adjusted to the free nucleon-nucleon scattering. The differences from cross sections calculated from the imaginary part of the Brückner G-matrix are minor [51] and influence little the observables of a heavy ion collision. For a derivation of this equation see [44,45].

The equation is solved by use of the testparticle method. Here the continuous one-body distribution function f at $t=0$ is represented by an ensemble of $n\cdot(A_p+A_t)$ pointlike particles. This is often viewed as an ensemble of n parallel events with A_p+A_t physical particles each, where A_p and A_t denote the number of nucleons in projectile and target, respectively. The l.h.s. of (1) can be regarded as the transport equation (Vlasov-equation) for a distribution of classical particles whose time evolution is governed by Hamilton's equations of motion.

$$\dot{\boldsymbol{p}}_i = -\frac{\partial\langle H\rangle}{\partial \boldsymbol{r}_i} \quad \text{and} \quad \dot{\boldsymbol{r}}_i = \frac{\partial\langle H\rangle}{\partial \boldsymbol{p}_i}\,, \tag{3}$$

The testparticles move due to their own, selfconsistently generated mean-field. The r.h.s. is taken into account by additional stochastic scattering similar to the collisions in cascade models [30,31].

More explicitly the test particle method corresponds to the replacement of the expectation value of a single particle observable

$$\langle O(t)\rangle = \int f(\boldsymbol{r},\boldsymbol{p},t) O(\boldsymbol{r},\boldsymbol{p})\, d^3r\, d^3p \tag{4}$$

by a Monte Carlo integration

$$\langle O(t)\rangle = \frac{1}{n(A_T+A_P)} \sum_{i=1}^{n(A_T+A_P)} O(\boldsymbol{r}_i(t),\boldsymbol{p}_i(t)) \tag{5}$$

where the $\boldsymbol{r}_i(t)$ and $\boldsymbol{p}_i(t)$ are points in phase space which are distributed according to $f(\boldsymbol{p},\boldsymbol{r},t)$, i.e.,

$$\begin{aligned} f(\boldsymbol{p},\boldsymbol{r},t) = \lim_{n\to\infty} &\frac{1}{n(A_T+A_P)} \\ &\times \sum_{i=1}^{n(A_T+A_P)} \delta(\boldsymbol{r}-\boldsymbol{r}_i(t))\delta(\boldsymbol{p}-\boldsymbol{p}_i(t)) \end{aligned} \tag{6}$$

It is evident that a large number n is necessary to avoid numerical noise. Predictions beyond the one-body level are not feasible although several attempts have been made to relate the (unphysical) numerical noise to physical fluctuations. In practice the number n lies in the range between 15 and 500 and one employs a grid to obtain a smooth phase space density distribution.

The numerical realization can be achieved in various ways. VUU uses a phase space sphere around each particle in order to determine f and a coordinate space sphere

to determine ρ and thus $U(\rho)$. This corresponds to a Lagrangian method. On the contrary, BUU uses a fixed grid corresponding to an Eulerian method in hydrodynamics. In both models collisions are treated in a parallel event method, only testparticles of the same events, i.e. the A_p+A_t test particles with the same index n, can collide. The Landau-Vlasov model determines f by the overlap of several Gaussians. The collisions are performed in a crossed-event (or full ensemble) method where all $n(A_p+A_t)$ may collide with each other particle with a scaled cross section.

For a solution of (1) proper boundary conditions have to be specified. In the case of heavy ion reactions, the test particles are distributed according to the density- and (Fermi-) momentum distribution of ground state nuclei. The latter are then boosted onto every other with the proper relative momentum. Initially the test particles are randomly distributed in a coordinate space sphere of the radius $R = 1.12A^{1/3}$ fm (where A is the atomic number of the nucleus) and in a momentum space sphere of the radius of the corresponding Fermi momentum.

One should keep in mind that the forces acting on the testparticles are calculated from the entire distribution including testparticles from all events, hence the n parallel events are not independent and event-by-event correlations cannot be analyzed within this one-body transport models. In the limit $n \to \infty$ the distribution of these propagated test particles at the time t represents the one-body distribution function at this time. Any one-body observable can be calculated by averaging the values weighted with the distribution function according to (5). Hence, VUU type models succeeded in the description of one-body observables like collective flow, stopping and particle spectra, but, fluctuations and correlations, such as the formation of fragments or the description of two-particle correlations in relativistic heavy ion collisions, are beyond the scope of a transport model based on a one–body distribution function [25,26]. Any fluctuation of the observables seen in the Monte Carlo simulation of the one–body distribution function is due to numerical noise and disappears in the limit of a infinite number of test particles.

B The quantum molecular dynamics approach

An approach which goes beyond a one-body description as explained above, is the Quantum Molecular Dynamics (QMD) model [41,23,32,8]. The QMD model is a n-body theory which simulates heavy ion reactions at intermediate energies on an event by event basis. Taking into account all fluctuations and correlations has basically two advantages: i) many-body processes, in particular the formation of complex fragments are explicitly treated and ii) the model allows for an event-by-event analysis of heavy ion reactions similar to the methods which are used for the analysis of exclusive high acceptance data.

The major aspects of the formulation of QMD will now be discussed briefly. For a more detailed description we refer to [8]. The particular realizations of this model will be discussed later.

1 Formal derivation of the transport equation

In QMD each nucleon is represented by a coherent state of the form (we set $\hbar, c = 1$) which are characterized by 6 time-dependent parameters, $\boldsymbol{r}_i$ and $\boldsymbol{p}_i$, respectively.

$$\phi_i(\boldsymbol{x}_i;t) = \left(\frac{2}{L\pi}\right)^{3/4} e^{-(\boldsymbol{x}_i-\boldsymbol{r}_i(t))^2/L}\, e^{i\boldsymbol{x}_i\boldsymbol{p}_i(t)}. \quad (7)$$

The parameter L, which is related to the extension of the wave packet in phase space, is fixed. The total n-body wave function is assumed to be the direct product of coherent states (7)

$$\Phi = \prod_i \phi_i(\boldsymbol{x}_i, \boldsymbol{r}_i, \boldsymbol{p}_i, t) \quad (8)$$

Note that we do not use a Slater determinant (with $(A_p+A_t)!$ summation terms) and thus neglect antisymmetrization. First successful attempts to simulate heavy ion reactions with antisymmetrized states have been performed for small systems [21,22]. A consistent derivation of the QMD equations of motion for the wave function under the influence of both, the real and the imaginary part of the G-matrix, however, has not yet been achieved. Therefore we will add the imaginary part as a cross section and treat them as in the cascade approach. How to incorporate cross sections into a antisymmetrized molecular dynamics is not yet known. This limits its applicability to very low beam energies.

The initial values of the parameters are chosen in a way that the ensemble of $A_T + A_P$ nucleons gives a proper density distribution as well as a proper momentum distribution of the projectile and target nuclei.

The equations of motion of the many-body system is calculated by means of a generalized variational principle: we start out from the action [37]

$$S = \int_{t_1}^{t_2} \mathcal{L}[\Phi, \Phi^*]dt \quad (9)$$

with the Lagrange functional $\mathcal{L}$

$$\mathcal{L} = \left\langle \Phi \left| i\hbar\frac{d}{dt} - H \right| \Phi \right\rangle \quad (10)$$

where the total time derivative includes the derivation with respect to the parameters. The Hamiltonian H contains a kinetic term and mutual interactions V_{ij}, which can be interpreted as the real part of the Brückner G-matrix supplemented by the Coulomb interaction. We will lateron describe the components of H in detail. The time evolution of the parameters is obtained by the requirement that the action is stationary under the allowed variation of the wave function. This yields an Euler-Lagrange equation for each parameter.

If the true solution of the Schrödinger equation is contained in the restricted set of wave functions $\phi_i(\boldsymbol{x}_i, t)$ (with parameters $\boldsymbol{r}_i, \boldsymbol{p}_i$) this variation of the action gives the exact solution of the Schrödinger equation. If the parameter

space is too restricted we obtain that wave function in the restricted parameter space which comes closest to the solution of the Schrödinger equation. Note that the set of wave functions which can be covered with special parametrizations is not necessarily a subspace of Hilbert-space, thus the superposition principle does not hold.

For the coherent states and a Hamiltonian of the form $H = \sum_i T_i + \frac{1}{2}\sum_{ij} V_{ij}$ (T_i= kinetic energy, V_{ij} = potential energy) the Lagrangian and the variation can easily be calculated and we obtain:

$$\mathcal{L} = \sum_i \left[-\dot{\boldsymbol{r}}_i \boldsymbol{p}_i - T_i - \frac{1}{2}\sum_{j\neq i}\langle V_{ik}\rangle - \frac{3}{2Lm}\right]. \tag{11}$$

Variation yields:

$$\dot{\boldsymbol{r}}_i = \frac{\boldsymbol{p}_i}{m} + \nabla_{\boldsymbol{p}_i}\sum_j \langle V_{ij}\rangle = \nabla_{\boldsymbol{p}_i}\langle H\rangle \tag{12}$$

$$\dot{\boldsymbol{p}}_i = -\nabla_{\boldsymbol{r}_i}\sum_{j\neq i}\langle V_{ij}\rangle = -\nabla_{\boldsymbol{r}_i}\langle H\rangle \tag{13}$$

with $\langle V_{ij}\rangle = \int d^3x_1\, d^3x_2\, \phi_i^*\phi_j^* V(x_1,x_2)\phi_i\phi_j$. These are the time evolution equations which are solved numerically. Thus the variational principle reduces the time evolution of the n-body Schrödinger equation to the time evolution equations of $6\cdot(A_P + A_T)$ parameters to which a physical meaning can be attributed. The equations of motion for the parameters $\boldsymbol{p}_i$ and $\boldsymbol{r}_i$ read

$$\dot{\boldsymbol{p}}_i = -\frac{\partial\langle H\rangle}{\partial \boldsymbol{r}_i} \quad \text{and} \quad \dot{\boldsymbol{r}}_i = \frac{\partial\langle H\rangle}{\partial \boldsymbol{p}_i}\,, \tag{14}$$

and show the same structure as the classical Hamilton equations, (3). The numerical solution can be treated in a similar manner as it is done in classical molecular dynamics [33–36]. Trial wave functions other than the gaussians in (7), yield more complex equations of motion for other parameters and hence the analogy to classical molecular dynamics is lost. If $\langle H\rangle$ has no explicit time dependence, QMD conserves energy and momentum by construction.

2 Description of the Hamiltonian

The nuclear dynamics of the QMD can also be translated into a semiclassical scheme. The Wigner distribution function f_i of the nucleon i can be easily derived from the test wave functions (note that antisymmetrization is neglected).

$$f_i(\boldsymbol{r},\boldsymbol{p},t) = \frac{1}{\pi^3\hbar^3}\mathrm{e}^{-(\boldsymbol{r}-\boldsymbol{r}_i(t))^2\frac{2}{L}}\mathrm{e}^{-(\boldsymbol{p}-\boldsymbol{p}_i(t))^2\frac{L}{2\hbar^2}} \tag{15}$$

and the total Wigner density is the sum of those of all nucleons. Hence the expectation value of the total Hamiltonian reads

$$\begin{aligned}\langle H\rangle &= \langle T\rangle + \langle V\rangle \\ &= \sum_i \frac{p_i^2}{2m_i} + \sum_i\sum_{j>i}\int f_i(\boldsymbol{r},\boldsymbol{p},t)\, V^{ij} \\ &\quad \times f_j(\boldsymbol{r}\,',\boldsymbol{p}\,',t)\, d\boldsymbol{r}\, d\boldsymbol{r}\,' d\boldsymbol{p}\, d\boldsymbol{p}\,'.\end{aligned} \tag{16}$$

The baryon-potential consists of the real part of the G-Matrix which is supplemented by the Coulomb interaction between the charged particles. The former can be further subdivided in a part containing the contact Skyrme-type interaction only, a contribution due to a finite range Yukawa-potential, and a momentum dependent part. $V^{ij} = G^{ij} + V^{ij}_{Yuk} + V^{ij}_{Coul} + V^{ij}_{mdi}$ consists of

$$\begin{aligned}V^{ij} &= G^{ij} + V^{ij}_{\mathrm{Coul}} \\ &= V^{ij}_{\mathrm{Skyrme}} + V^{ij}_{\mathrm{Yuk}} + V^{ij}_{\mathrm{mdi}} + V^{ij}_{\mathrm{Coul}} \\ &= t_1\delta(\boldsymbol{x}_i-\boldsymbol{x}_j) + t_2\delta(\boldsymbol{x}_i-\boldsymbol{x}_j)\rho^{\gamma-1}(\boldsymbol{x}_i) \\ &\quad + t_3\frac{\exp\{-|\boldsymbol{x}_i-\boldsymbol{x}_j|/\mu\}}{|\boldsymbol{x}_i-\boldsymbol{x}_j|/\mu} + \\ &\quad + t_4\ln^2(1+t_5(\boldsymbol{p}_i-\boldsymbol{p}_j)^2)\delta(\boldsymbol{x}_i-\boldsymbol{x}_j) + \frac{Z_iZ_je^2}{|\boldsymbol{x}_i-\boldsymbol{x}_j|}\end{aligned} \tag{17}$$

Z_i, Z_j are the charges of the baryons i and j. The real part of the Brückner G-matrix is density dependent, which is reflected in the expression for G^{ij}. The expectation value of G for the nucleon i is a function of the interaction density ρ^i_{int}. It is indeed this quantity which relates the number density to the energy content of nuclear matter.

$$\rho^i_{\mathrm{int}}(\boldsymbol{r}_i) = \frac{1}{(\pi L)^{3/2}}\sum_{j\neq i}\mathrm{e}^{-(\boldsymbol{r}_i-\boldsymbol{r}_j)^2/L} \tag{18}$$

Note that the interaction density has twice the width of the single particle density. Moreover, the particles do not interact with themselves. This is different compared to VUU-type models because in QMD explicit N–N interactions are treated, hence the force acting on a particle at the position $\boldsymbol{r}$ depends on the exact positions of all other particles, whereas the density employed in the one-body theories (6) depends on the average number of nucleons in the vicinity of the test particle only.

It should be noted that the width L of the distribution function determines the interaction range of the particle and influences the density distribution of finite systems. Therefore its value has to be adopted to reasonable interaction ranges of the strong interaction.

The momentum dependence V^{ij}_{mdi} of the N–N interaction, which may optionally be used in QMD, is fitted to experimental data [38,39] on the real part of the nucleon optical potential [6,41,40], which yields

$$U_{mdi} = \delta\cdot\ln^2\left(\varepsilon\cdot(\Delta\boldsymbol{p})^2+1\right)\cdot\left(\frac{\rho_{int}}{\rho_0}\right) \tag{19}$$

These measurements have been superseded recently by new data [42] and thus a new parametrization has been advanced [43].

The potential part of the equation of state (we will discuss this concept in the next subsection in more detail) resulting from the convolution of the distribution functions f_i and f_j with the interactions $V^{ij}_{\mathrm{Skyrme}} + V^{i,j}_{\mathrm{mdi}}$ (local interactions including momentum dependence) then reads:

$$U = \alpha\cdot\left(\frac{\rho_{int}}{\rho_0}\right) + \beta\cdot\left(\frac{\rho_{int}}{\rho_0}\right)^{\gamma} + \delta\cdot\ln^2\left(\varepsilon\cdot(\Delta\boldsymbol{p})^2+1\right)\cdot\left(\frac{\rho_{int}}{\rho_0}\right) \tag{20}$$

Here it should be noted that due to the definition of ρ_{int} (18) no mean-field potentials (as e.g. (2) for VUU) show up in the calculation of the equations of motion (14) of QMD but a sum of two (and three) body interactions (see 18). Hence energy and momentum are – in contrast to single VUU 'events' – strictly conserved in each event.

The Coulomb interaction cannot be treated for infinite matter, since this leads to diverging terms. In the first versions of QMD no explicit treatment of the isospin is performed and the charges are replaced by effective charges, i.e. all nucleons had been attributed the effective charge $Z = (Z_{proj.} + Z_{targ.})/(A_{proj.} + A_{targ.})$. IQMD (we will later come to that) and other more recent versions use the real baryon charges.

The parameters μ and $t_1...t_5$ are adjusted to fit the real part of the G-matrix and to describe the properties of finite nuclei.

3 The relation to the nuclear equation of state

One strong motivation for the numerical simulation of heavy ion reactions is the possibility to investigate effects of the underlying nuclear equation of state on the dynamics and final states of these collisions. QMD is a model for non-equilibrium dynamics with mutual interactions among the constituents and therefore does not contain any parametrization of the nuclear equation of state in terms of an explicit relation between number density, temperature and the energy density. In equilibrium and in the thermodynamic limit ($n \to \infty$), however, such a functional relation can be deduced from the nucleon-nucleon potentials and the cross-sections employed in the model.

For the description of the energy per nucleon as a function of density (assuming $T = 0$) usually Skyrme type parametrizations (see eq. (2)) are used. This ansatz is phenomenological and can be derived for the case $\gamma = 2$ from the assumption that the particles interact with each other with two- and threebody contact forces. It is generalized to effective higher order contact terms by setting $\gamma > 1$ to be a real number. This generalized ansatz uses three parameters α, β, γ; two of them are fixed by the constraint that the total energy should have a minimum at the saturation density $\rho = \rho_0$ with a value of $E/A = -16$ MeV which corresponds to the the volume energy in the Bethe-Weizsäcker mass formula. Together with the condition that a free particle has no binding energy (which is automatically fulfilled within this ansatz) there remains one degree of freedom. The third parameter is fixed by the nuclear compressibility, which is the second derivative of the energy at the minimum with respect to the density:

$$\kappa = 9\rho^2 \frac{\partial^2}{\partial \rho^2} \left(\frac{E}{A} \right) \tag{21}$$

Two different equations of state are commonly used: A hard equation of state (H) with a compressibility of κ =380 MeV and a soft equation of state (S) with a compressibility of κ =200 MeV [17,27].

To derive an equation of state from the interactions used in (18) we have to convolute the potentials with the distribution functions assuming an infinite homogeneous distribution. In this limit the $V_{\rm Skyrme}$ and $V_{\rm Yuk}$ become functions of the constant density only. The interaction density of (18) as used in (20) can be replaced by the position independent nuclear matter density. The integration over the relative momenta of infinite nuclear matter Fermi distributions finally turns into a density dependence of the momentum dependent interaction. This allows us to obtain the compressional part of the nuclear equation of state, which depends on the density only. The parameters of the interactions in (18) can therefore be chosen that way that a hard or soft eos is obtained for the infinite matter case. It should again be noted that the parameters of the potentials allow a relation to the nuclear equation of state (eos) but that the microscopic description works as well for systems far off from equilibrium where no eos can be defined.

The interaction range parameter L influences the interaction density (18) for finite systems. For (homogeneous) infinite nuclear matter the density (and thus the potential energy) do not depend anymore on the extension of the gaussian wavepackets. Thus, the equation of state of infinite nuclear matter is independent of L. In finite matter E/A also depends on L. Thus even two parametrizations which yield the same eos may produce different results for the reaction of two heavy ions. Therefore we have to adjust L to have reasonable surface properties. In order to allow a physical interpretation L should be in the order of the size one expects for the range of the nuclear interaction. There exists a range of values for L, which allows to fix these properties. Larger values of L increase the effective range of the interaction and thus lead to some smearing of fluctuations, which are stronger for more located wavepackets (small values of L).

Hence, the nuclear equation of state can only be defined as the bulk properties in the limit of an infinite system: The concept of the nuclear equation of state as discussed here does only make sense for large macroscopic systems in (at least local) equilibrium, while the ansatz with mutual interactions has no restrictions with respect to the size and is therefore also applicable for finite systems far off equilibrium. The time evolution of the non-thermal system of two reacting heavy ions is completely determined by the two-body potentials and the scattering cross sections, respectively.

In QMD the parameters $t_1...t_5$ are uniquely related to the corresponding values of $\alpha, \beta, \gamma, \delta$ and ϵ which serve as input. The standard values of these parameters can be found in Table 1.

4 Inclusion of collisions

As stated above the imaginary part of the G-matrix acts like a collision term. In the QMD simulation we restrict ourselves to binary collisions (two-body level). The collisions are performed in a point-particle sense in a similar way as in VUU or cascade: Two particles collide if their minimum distance d, i.e. the minimum relative distance of the centroids of the Gaussians during their motion, in

Table 1. Parameter sets for the nuclear equation of state used in the QMD model. S and H refer to the soft and hard equations of state, M refers to the inclusion of momentum dependent interaction

	α (MeV)	β (MeV)	γ	δ (MeV)	$\varepsilon\left(\frac{c^2}{\mathrm{GeV}^2}\right)$
S	-356	303	1.17	—	—
SM	-390	320	1.14	1.57	500
H	-124	71	2.00	—	—
HM	-130	59	2.09	1.57	500

their CM frame fulfills the requirement:

$$d \leq d_0 = \sqrt{\frac{\sigma_{\mathrm{tot}}}{\pi}}, \qquad \sigma_{\mathrm{tot}} = \sigma(\sqrt{s},\ \mathrm{type}). \tag{22}$$

where the cross section is assumed to be the free cross section of the regarded collision type ($N-N$, $N-\Delta$, ...).

Beside the parameters describing the N–N potential, the cross sections constitute another major part of the model. In principle, both sections of parameters are connected and can be deduced from Brückner theory. QMD-calculations using consistently derived cross-sections and potentials from the local phase space distributions have been discussed e.g. in [72]. Such simulations are time-consuming since the cross-sections and potentials do explicitly depend on the local phase space population.

Within the framework of using free cross section one may parametrize the cross section of the processes to fit to the experimental data if available. For unknown cross sections isospin symmetry and time reversibility is assumed.

Alternatively, cross-sections may be obtained from theoretical considerations. For one particular QMD-version the one boson exchange model has been employed for this purpose. This has the advantage to have a first handle for the description of cross sections in the nuclear medium.

If two particles scatter, the direction of the final momenta will be distributed randomly in such a way that the distribution of many identical collisions corresponds to the measured cross section. For elastic scattering the distribution is taken from [47]:

$$\frac{\mathrm{d}\sigma_{\mathrm{el}}}{\mathrm{d}\Omega} \sim \exp(A(s)\cdot t), \tag{23}$$

where t is $-q^2$, the squared momentum transfer (which also includes the information on the polar angle) and $\sqrt{s}$ is the c.m. energy in GeV.

It should be noted that the presented treatment of the collisions may cause problems with causality since the particles can interact immediately at a distance. The collision information is given to both particles at the same time when they are at closest position. It should also be noted that the time order of the collisions is determined in a common system of all particles. The evolution of the system is propagated with one common clock. As it has been already pointed out by Kodama et al. [48] the time ordering is not unique. Thus the choice of the common referential system may influence the observables. Normally a system is chosen where the relative velocities with respect to that system are as small as possible. Thus BQMD used the nucleus-nucleus CM system as referential system and VUU and IQMD use the nucleon-nucleon CM system. The choice of the Lab system as referential system would e.g. cause for the system Au(1AGeV)+Au b = 3fm, hard eos, an enhancement of the flow (in IQMD p_x^{dir} rises from 98 ± 3 MeV/c to 110 ± 3 MeV/c in the Lab system) and a reduction of the pion number (in IQMD N_π falls from 64 ± 1 to 60 ± 1 in the Lab system).

Also the choice of the minimum distance point as collision point can be motivated within this respect. An earlier collision (e.g. at the point when the distance is sufficient to fulfill the distance condition) could cause stronger acausalities. It will also reduce the mean free path and thus enlarge stopping and flow [49].

5 Pauli blocking due to Fermi statistics

The cross section is reduced to an effective cross section by the Pauli-blocking. For each collision the phase space densities in the final states are checked in order to assure that the final distribution in phase space is in agreement with the Pauli principle ($f \leq 1$). Phase space in QMD is not discretized into elementary cells as in one-body models like VUU, in order to obtain smooth distribution functions the following procedure is applied: The phase space density f_i' at the final states $1'$ and $2'$ is measured and interpreted as a blocking probability. Thus, the collision is only allowed with a probability of $(1-f_1')(1-f_2')$. If the collision is not allowed the particles remain at their original momenta.

The Pauli blockers of VUU and QMD show efficiencies of about 94-96 %, i.e. a single ground state nucleus with Fermi momentum would show a blocking rate of this amount. In order to reduce the noise of spurious collisions in ground state nuclei additional conditions allow a nucleon only to collide with a nucleon of the other nucleus or with a nucleon that has already undergone a collision. Nevertheless the problem of Pauli blocking causes a limitation of the calculated system to have not less incident energy than about the Fermi energy.

C Numerical structure

The QMD model consists of three major parts, namely i) the **initialisation** of projectile and target, ii) the **propagation** of nucleons, resonances and newly produced particles due to their mutual potential interactions, and iii) the **hard collisions** according to the energy dependent cross section for the various channels together with the **Pauli-blocking**.

For the propagation the description of the **potential** (or to be more exact of the real part of the Brückner G-matrix) is of crucial importance.

The solution of the transport equations for the N-body distribution function is done in the following way:

1. Projectile and target are initialized. For each of these nuclei the nucleons initialized according to a distribution $f(r, p, t = 0)$. This distribution is essentially constrained by the requirement to reproduce the ground state properties of the two nuclei, i.e. radii, binding energies.
2. The particles are propagated using Hamilton's equations of motion (14) with a given Hamiltonian $\langle H \rangle$.
3. Two particles close in coordinate space may perform a collision. The particles change their momenta respecting the Pauli principle.

The input into the program may be subdivided into three classes of parameters

Reaction parameters: projectile and target masses (and charges), bombarding energy, impact parameter. They define the whole kinematics of a single event.

Physics Parameters: interaction range, potential parameters, in medium cross sections and decay widths, etc. They correspond to a detailed description of interactions and may be changed within a reasonable range. Finally their deduction is a particular goal of the comparison between calculation and experiment.

Technical parameters: time step size, initial distance, cutoff parameters, maximum collision distance, etc. They are used to perform effective calculations on a computer. The observables should not depend on them.

If all these parameters are fixed the calculation of a single event can be performed in the following way:

- initialize projectile and target nuclei in their "ground states" as mentioned above,
- propagate the constituents of the system according to their mutual potential and hard scattering interactions, this includes
  - calculation of interaction densities, forces and the Hamiltonian
  - propagation of all particles according to Hamilton's equation of motion
  - perform all collisions within this time step. Decide for each collision whether its final state is Pauli-blocked. If this is the case: keep momenta of collision partners unchanged, otherwise change momenta according to the angular distribution of this particular channel.
- output of information (coordinates, momenta, scattering partners, ...) about the intermediate reaction stages and output of the final phase-space configuration (which would correspond to the freeze-out configuration in a thermal picture).

This procedure is repeated until sufficient statistics, i.e. a large number of independent events, is obtained.

This principal structure is common for all QMD realizations, which differ, however, in details and the initialisation of projectile and target. In the following we will study the influence of these differences on observable and nonobservable quantities.

III Description of particular QMD model realizations

The original QMD [19,23] program was developed further to include momentum dependent interactions [41,32].

A BQMD

The original QMD has been rewritten by Bohnet et al. [51] for the purpose of studying low energy fragmentation data. This program has been dubbed BQMD since it was designed for describing the proper binding of a nucleus in order to describe fragmentation processes [52–55]. An improvement on the stability against artificial particle evaporation has been achieved in BQMD by a procedure explained below which causes fluctuations of the energy around the mean value by 2 MeV/nucleon.

1 Initialisation in BQMD

In BQMD the nucleons are distributed within a sphere with a Wood-Saxon-type density profile. (The original QMD used a sphere for the distribution of the centroids of the Gaussians.) The maximum Fermi-momentum is limited by the local binding energy of the nucleon in order to keep all particles bound. By this procedure, however, the mean kinetic energy of the particles is lowered to about 10 to 12 MeV/nucleon. The ground state central density is assumed to be $\rho_0 = 0.15$ fm^{-3}. The Gaussian width for the interactions are chosen to be $L = 4.33$ fm^2. The binding energy as given in the Weizsaecker mass formula is reproduced from Lithium up to the heaviest nuclei [8]. As already seen in Fig. 10 of [8] this particular version suffers from fluctuations of the rms radius. The consequences will be discussed later.

2 Potentials in BQMD

The range and the strength of the Yukawa potential in BQMD has been chosen to describe the surface of the nucleus best. In order to keep the nuclear equation of state and the binding energy independent of the Yukawa interactions and to keep the binding energy at its experimental value, the coupling constant t_1 of the Skyrme-type two body interaction. is modified according to [8]

$$t_1^i(i)\rho(\boldsymbol{r}_{i0}) = t_1\rho(\boldsymbol{r}_{i0}) - \sum_j U_{ij}^{Yuk}\,. \tag{24}$$

Note that the Skyrme and Yukawa coupling constants are different for each particle here. With this procedure the validity of Newtons theorem *actio = reactio* can be assured on the ensemble average only, which also leads to violation of energy conservation in single events. The energy fluctuates about 2 MeV/nucleon around the mean value [8]. The range of the Yukawa-potential is chosen as 1.5 fm.

3 Collision term in BQMD

BQMD has in common with the original QMD that it uses nucleons and deltas only. The employed cross sections have been parametrized by Cugnon [47]. All nucleons interact with the same average cross section without distinction in isospin. The elastic cross section is given by a constant value of 55 mb for collisions with $\sqrt{s} \leq 1.8993$ GeV and for higher energies by the parametrization:

$$\sigma_{el}(mb) = \frac{35}{1 + 100 \cdot (\sqrt{s}/GeV - 1.8993)} + 20 \qquad (25)$$

The inelastic cross section $NN \to N\Delta$ is zero for $\sqrt{s} \leq 2.015$ GeV and for higher values by the parametrisation

$$\sigma_{in}(mb) = \frac{20x^2}{0.15 - x^2} \qquad x = \sqrt{s}/GeV - 2.015 \qquad (26)$$

The angular distribution of the collisions is described by $\frac{\mathrm{d}\sigma_{\mathrm{el}}}{\mathrm{d}\Omega} \sim \exp(A(s)\ t)$ with

$$A(s) = 6\,\frac{(3.65\ (\sqrt{s}/GeV - 1.8766))^6}{1 + (3.65\ (\sqrt{s}/GeV - 1.8766))^6}. \qquad (27)$$

B IQMD

The Isospin-QMD (IQMD) [58,49] treats the different charge states of nucleons, deltas and pions explicitly, as inherited from the VUU model. IQMD has been used for the analysis of collective flow effects of nucleons [58,63–65] and pions [60–62]. Comparisons to experimental data with this model have been presented in [66–68]. As it has been developed from the VUU-model, its coding is therefore independent of the original QMD. The isospin degrees of freedom enter into the cross sections (here cross sections of VUU [17] similar to the parametrizations of VerWest and Arndt [59] have been taken, see also [62]) as well as in the Coulomb interactions. The elastic and inelastic cross sections for proton-proton and proton-neutron collisions used in IQMD are shown in Fig. 1. The cross section for neutron-neutron collisions are assumed to be equal to the proton-proton cross sections.

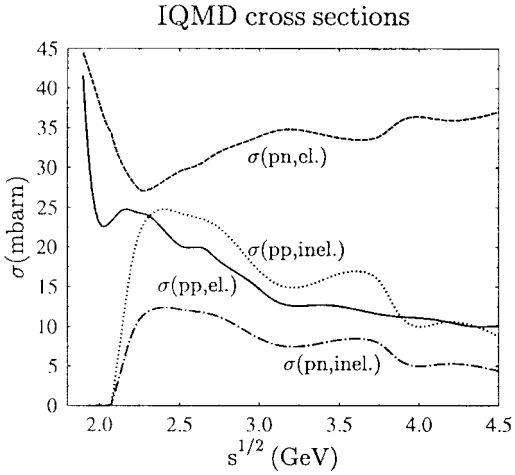

Fig. 1. The elastic and inelastic cross sections for proton-proton (pp) and proton-neutron (pn) used in IQMD. The neutron-neutron cross section is assumed to equal to the pp case. The total cross section is equal to the sum of elastic and inelastic cross section

1 Potentials used in IQMD

The IQMD-model offers rather stable density distributions and good energy conservation, however for the price of nucleon evaporation and and improper binding energies ($E_{bind} \approx 4 - 5$ MeV/nucleon for heavy nuclei instead of 8 MeV/nucleon).

In addition to the use of the explicit charge states of all baryons and mesons a symmetry potential between protons and neutrons corresponding to the Bethe-Weizsäcker mass formula has been included

$$V_{sym}^{ij} = t_6 \frac{1}{\varrho_0} T_{3i} T_{3j} \delta(\boldsymbol{r}_i - \boldsymbol{r}_j) \quad t_6 = 100\,\mathrm{MeV} \qquad (28)$$

where T_{3i} and T_{3j} denote the isospin projections of particles i and j. Other baryonic potentials like V_{Skyrme}^{ij} and V_{mdi}^{ij} are defined isospin-independent like in all other flavors. The Yukawa potential in IQMD V_{Yuk}^{ij} is very short ranged ($\mu = 0.4$ fm in contrast to $\mu = 1.5$ fm in BQMD) and weak. The modification of the α term of the static potential is done in an particle independent way. As in BQMD this corresponds to the interpretation that an additional term in the Skyrme ansatz which is proportional to $(\nabla\rho)^2$ can be expanded in first order to a term linear in density (which reduces α effectively) plus Yukawa potentials. Additional attractive Yukawa forces hence modify the EOS (and therefore the α term has to be modified to obtain the same EOS). Yukawa forces stabilize the nuclei because of the increase of the interaction range as compared to a δ-like Skyrme-potentials. Thus nucleons notice earlier that they will arrive at the surface and are more effectively decelerated as without this potential. In addition the fluctuations are reduced.

2 Pions in IQMD

Free pions are moving under the influence of the Coulomb interactions. Pions may be produced by the decay of a Δ-resonance and may be reabsorbed by a nucleon forming a delta again. IQMD and HQMD, which will be described in the next section, differ concerning the pion production in the production cross sections (HQMD uses cross sections based on the one boson exchange model), the included resonances (HQMD contains additionally N^* and $NN \to \Delta\Delta$ collisions) and the angular distribution of inelastic collisions (HQMD has more realistic non-isotropic distributions obtained from OBE calculations which are not present in original IQMD). Recent updates of IQMD calculating the pion production (e.g. [61,62]) also use the

inelastic angular distributions of HQMD. The effect of this modification on nucleonic observables is quite small.

3 Initialisation in IQMD

The most important difference to BQMD is the initialisation. In IQMD the centroids of the Gaussians in a nucleus are randomly distributed in a phase space sphere ($r \leq R$ and $p \leq p_F$) with $R = A^{1/3} \cdot 1.12$ fm corresponding to a ground state density of $\rho_0 = 0.17\ \mathrm{fm}^{-3}$. The Fermi momentum p_F depends on the ground state density. For $\rho_0 = 0.17\ \mathrm{fm}^{-3}$ it has a value of about $p_F \approx 268$ MeV/c. While, as said, in BQMD the maximum momentum is determined by the local binding energy (which causes an effective reduction of the total Fermi energy to about 10 – 12 MeV), in IQMD the momenta are uniformly distributed within a momentum sphere $p \leq p_{Fermi} \approx 268$ MeV/c without further local constraints. Therefore it may happen that nucleons close to the surface, where the local potential energy is low, are unbound initially. This possibility is not given in BQMD or HQMD. It gives, however, a reduced binding energy per nucleon as compared to the Weizsäcker mass formula. Hence the initialized nuclei are less stable against spurious particle evaporation as compared to BQMD. On the other hand this ansatz makes available the full Fermi-energy calculated from the Skyrme ansatz. The full Fermi pressure yields (as compared to BQMD) a stronger stability of the density profile against vibration modes. Finally it should be noted that IQMD performs a Lorentz contraction of the nucleus coordinate distribution which is not present in BQMD and which becomes important for higher energies $E/nucleon > 1$ GeV.

4 Interaction range

As it has already been stated, the Gaussian width can be regarded as a description of the interaction range of a particle. Its influence disappears for infinite nuclear matter whereas for finite systems it may play a non negligible role.

In IQMD the Gaussian width can be used as an optional input parameter. The default version of uses a system dependent Gaussian width while BQMD uses $L = 4.33\,\mathrm{fm}^2$ independent of the system size. The system dependence of L in IQMD has been introduced in order to obtain maximum stability of the nucleonic density profiles. As an example for Au+Au a value of $L = 8.66\,\mathrm{fm}^2$ is choosen, for Ca+Ca and lighter nuclei $L = 4.33$.

C HQMD

HQMD is an upgrade of QMD which combines optional features of BQMD and IQMD. It does not remedy the shortcomings of BQMD and IQMD, but allows to study the influence of the different modules on physics results. In addition, higher resonances (the $N^*(1440)$), free pions and the proper isospin coupling have been incorporated by Huber et al. [56]. The isospin degrees of freedom play an important role especially for the particle production. The employed inelastic cross sections $NN \to NN^*, N\Delta$ and $\Delta\Delta$ have been calculated within an one-boson exchange model (OBE). Also the angular distribution of the inelastic reactions was calculated and parametrized in the following way:

$$\frac{\mathrm{d}\sigma_{\mathrm{in}}}{\mathrm{d}\Omega} \sim a(s)\ \exp(b(s) \cdot \cos\theta) \quad , \tag{29}$$

$a(s)$ and $b(s)$ are functions of $\sqrt{s}$ and vary in their definition for different intervals of $\sqrt{s}$ (see Table 2). θ is the polar angle. It should be noted that VUU, BUU and IQMD (in its older version) assumed isotropic scattering for the inelastic channels which causes differences in the flow at higher energies. For elastic collisions a new parametrisation [57] has been used which can be taken from Table 3.

In addition the numerical propagation routines have been changed to a higher accuracy. A 4th order Runge-Kutta propagation scheme allows an energy conservation of about 1 per mille. The Yukawa interaction has been suppressed.

This upgrade of QMD which has been dedicated to the question concerning the meson production. It is quoted as HQMD because it contains higher resonances.

HQMD offers the possibility to choose between the two initialisation modes of BQMD and IQMD. Moreover one can choose between the different parametrizations of the cross section as described above: the cross section parametrization used in IQMD and that used in BQMD. It was checked that it reproduces the results obtained with BQMD and with IQMD if the corresponding subroutines are used. Therefore it may be directly used to analyse the effects of the different ingredients in the QMD flavours.

D Other flavours

There exist several other flavours of QMD. Peilert et al. use an extension of QMD with additional implementation of a so-called Pauli potential [46]. These models use a strong repulsive potential which depends on the distance of the particles in phase space. It is effective in momentum- and in configuration space and prevents two identical particles from coming too close in phase-space. Its parameters have been adjusted to the temperature- and density-dependence of the energy per particle of an ideal Fermi-gas [69,70]. With aid of such a potential self-consistent nuclear ground states for nuclei with N neutrons and Z protons as well as for infinite nuclear matter can be constructed by searching for the minimum in the multi-dimensional potential-energy surface of N neutrons and Z protons. The nucleons carry their proper Fermi-momentum, however due to the momentum-dependence of the Pauli-potential, their velocities (=kinetic momenta $\partial H/\partial p$) vanish in the ground state. This can be interpreted as a first approximation to antisymmetrization in finite nuclei on the two-body level. However one should note that for the scattering of individual nucleons a Pauli potential and antisymmetrisation yield different effects.

Table 2. $a(s)$ and $b(s)$ as functions of the c.m. energy

$x = \sqrt{s}$ (GeV)	a (fm)	b
2.104 – 2.12	$294.6\ (x-2.014)^{2.578}$	$19.71\ (x-2.014)^{1.551}$
2.12 – 2.43	$\frac{0.01224}{(x-2.225)^2+0.004112}$	$19.71\ (x-2.014)^{1.551}$
2.43 – 4.50	$(2.343/x)^{43.17}$	$33.41\ \arctan(0.5404\ (x-2.146)^{0.9784})$

Table 3. Elastic cross section parametrization used in QMDRKNC and HQMD as a function of the relative momentum in the CM-frame

$x = \lvert\Delta\boldsymbol{p}(CM)\rvert/1$ GeV	σ_{el}(mb) for pp, nn	σ_{el} (mb) for pn
$x < 0.8$	$23.5 + 1000 \cdot (0.7-x)^4$	$33 + 196 \cdot \lvert 0.95-x\rvert^{2.5}$
$0.8 < x < 2$	$1250/(x+50) \quad - \quad 4\cdot(x-1.3)^2$	$31/\sqrt{x}$
$2 < x$	$77/(x+1.5)$	$77/(x+1.5)$

Konopka et al. generalized this concept by treating collisions of Gaussians instead of point particles as it is the case in all other QMD versions. For the sake of numerical feasibility the cross section has to be assumed as constant. This model has been utilized for analyses of the FOPI-data at lower energies [71]. The basic differences in the observables calculated with the Pauli-QMD and with IQMD can be explained by the use of a isotropic 41 mb cross section in the Pauli-potential QMD. However, one should stress that the Pauli-potential has - due to the strong momentum dependent potential - a different physical input as compared to all flavours discussed and hence a detailed comparison is not intended in this paper.

Further studies with QMD have been done by Jaenicke et al. who replaced potentials and cross sections of BQMD by those calculated from a Brücker G-matrix [72]. Comparison of experimental data with this model has been performed by the FOPI-collaboration [68].

Lehmann and Puri extended HQMD by including a relativistic covariant propagation scheme of the RQMD-type. The physical inspiration of the scheme was taken from the RQMD -model of Sorge [74], which originally was footed on the IQMD and vastly extended for the description of high energy collisions in the potential and the collision parts. Similarly, the RQMD of Lehmann and Puri is an numerical extension of the HQMD model. The inclusion of a covariant treatment of initialisation, Pauli-blocking and potentials yield at high energies ($E/A > 1$GeV) some differences to the 'nonrelativistic' HQMD which are described in [75,76]. The relativistic and the nonrelativistic version agree at low beam energies. Hence this program allows a systematic investigation from very low energies to very high energies. The required computing time, however, is one order of magnitude higher.

Kaon production has been intensively studied [80] using a modified version of HQMD. The differences are the neglect of free pions and the parametrization of the inelastic cross sections where only the reaction channel $NN \rightarrow N\Delta$ has been employed. Differences in the kaon production between this version and IQMD have been discussed in [73].

IV Numerical test and results

The above discussed QMD versions allow for simulations of heavy ion collisions up to $\approx$ 2 GeV/nucleon. Above this energy higher resonances, which are not included in the models under consideration become more and more important. The model gives detailed information about all one-body observables, such as single particle spectra, and many-body observables, such as particle correlations and fragment formation, on an event-by-event basis. Thus the structure of these theoretical data is analogous to experimental data. The independent development of BQMD and IQMD including different model assumptions lead to different results in some cases. In this section, we therefore compare several QMD versions with particular attention to some standard observables. It is demonstrated that most of the differences are related to the different treatment of the initialisation of the two colliding nuclei.

1 Rapidity distributions

A quantity, which is crucially related to the possible formation of a thermally equilibrated source is the rapidity distribution of baryons.

Figure 2 shows the rapidity distribution dN/dy of nucleons in the reaction Au+Au, b = 3 fm at 1 GeV/nucleon incident energy. IQMD (squares, dotted line), BQMD (circles, full line) and VUU calculations (triangles, dashed line) using a hard equation of state without momentum dependent interaction give quite similar results. BQMD shows a slightly broader distribution than IQMD and VUU. As it has been already stated in [41] the rapidity distribution depends strongly on the collision term and only slightly on the used nucleonic potentials. From this we can conclude that the hard collisions do not lead to large differences.

The remaining differences of about 40 units at midrapidity divides up as follows (the statistical error of each of the midrapidity dN/dy values amount to about 10-15 units): The change from large to small width enhances the value by about 20 units, whereas the different cross sections contribute a lowering by 30 units when switching

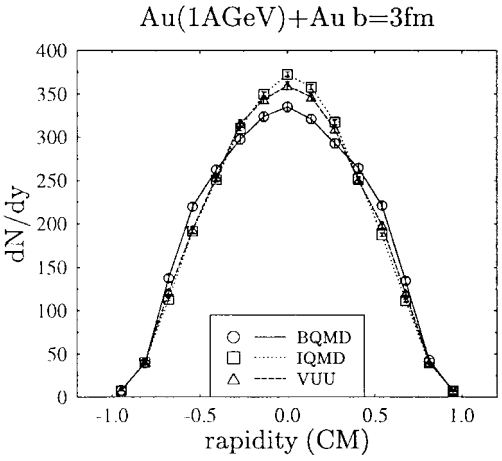

Fig. 2. Rapidity distributions dN/dy of nucleons in the reaction Au(1 GeV/nucleon)+Au, b=3fm for VUU, IQMD and BQMD. In all calculations a hard equation of state without momentum dependent interactions has been used

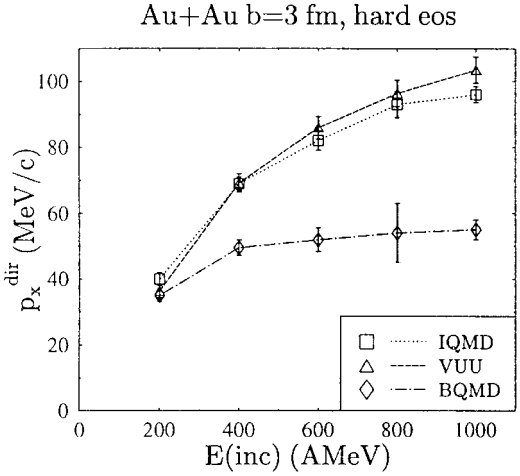

Fig. 3. Excitation function of the system Au+Au at $b = 3$fm impact parameter obtained with BQMD, IQMD and VUU in their default versions

from IQMD to BQMD. The BQMD initialisation lowers by about 20 units and the Yukawa potential in BQMD reduces by about 10 units.

At lower bombarding energies the dynamics is no longer dominated by the hard collisions and the nucleon potential becomes more important. At 150 MeV/nucleon, the rapidity distributions exhibit some larger differences between the two QMD version used. This, however, is due to the inclusion of Yukawa forces in BQMD. The results look more alike if this term is omitted in both calculations. The dN/dy at midrapidity reaches about 11% smaller values in BQMD, which are decomposed as follows: 7% enhancement due to the interaction range, 9% reduction due to the cross sections, 5% reduction due to Yukawa, and a slight reduction ($\approx 2\%$) due to different initialisations.

2 Transverse flow

Let us now focus on an observable whose investigation is strongly motivated by its dependence on the nuclear equation of state [4,27,32] (besides its dependence on the collision term and on the centrality), namely the transverse flow in plane. This variable turns out to be extremely sensitive to a lot of parameters as we will see. The amount of transverse flow created in heavy ion reactions is known as a measure of the pressure built up during the reaction and it thus can provide information about the underlying equation of state.

Figure 3 compares the excitation functions of flow for VUU, IQMD and BQMD with their default width parameters $L = 8.66\,\mathrm{fm}^2$ and $L = 4.33\,\mathrm{fm}^2$ respectively. It is found that VUU and IQMD show a similar behaviour with a rise of the flow up to 1 GeV incident energy (which is also in good agreement with experimental data) while BQMD shows rather weak rise of the flow. This weak rise is in disagreement with experimental flow data. The reasons of the differences between BQMD and IQMD shall be briefly investigated.

The transverse flow is not only sensitive to the repulsion of the compression zone formed by excited nuclear matter, but also to surface properties, such as the range of the nuclear interaction. This quantity may be varied within the QMD approach in two different ways:

The range of the optional Yukawa force in QMD is an adjustable parameter, it can be used to stabilize the width of the nuclear surface of a given density profile. The width parameter L of the gaussians serves as an effective interaction range as well. It should be noted that a change of the interaction range also changes the density gradient in inhomogeneous systems (this can be demonstrated by regarding the density profile of a 'box') and therefore directly enters into the gradient of the potential. It was found that default BQMD calculations with a Yukawa potential yielded a directed transverse momentum, p_x^{dir} which is about 10 MeV/c higher than for calculations where only the Skyrme interaction is used. This is due to the fact that a finite range Yukawa smears out the potential gradient more than a δ-function and hence reduces the force in transverse direction.

In IQMD the inclusion of Yukawa forces does not give significant effects on the nucleonic flow. It should however be noted, that in IQMD the range of the Yukawa force is smaller (0.4 fm as compared to 1.5 fm of BQMD) and that actio=reactio is respected for the two-body interactions.

Both models agree in the observation that a broadening of the Gaussian width L reduces the flow. This also corresponds to the fact that the density gradient to the high density region is smeared out.

The influence of the interaction range on the flow can be studied in Fig. 4 which compares IQMD results of the flow for $L = 8.66\,\mathrm{fm}^2$ and $L = 4.33\,\mathrm{fm}^2$. In IQMD the default value for Au+Au is chosen to be $L = 8.66\,\mathrm{fm}^2$. A smaller interaction range enhances the flow value by about 10 MeV/c at 400 AMeV and by 20 MeV/c at 1 AGeV. A further difference caused by the interaction range is the density of the saturation of the potential, i.e.the density where the potential supports maximum stability of the

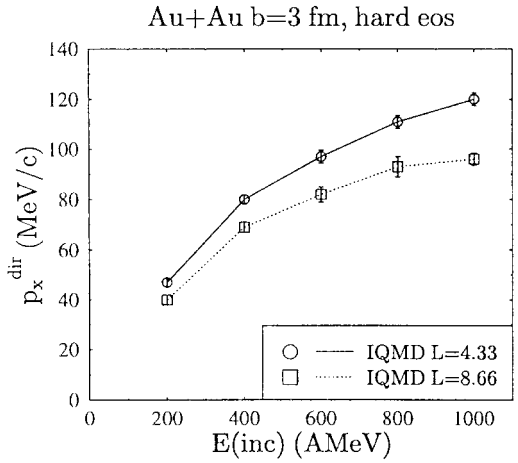

Fig. 4. Excitation function of the system Au+Au at $b = 3$ fm impact parameter obtained with IQMD using the width of $L = 4.33\,\mathrm{fm}^2$ and $L = 8.66\,\mathrm{fm}^2$

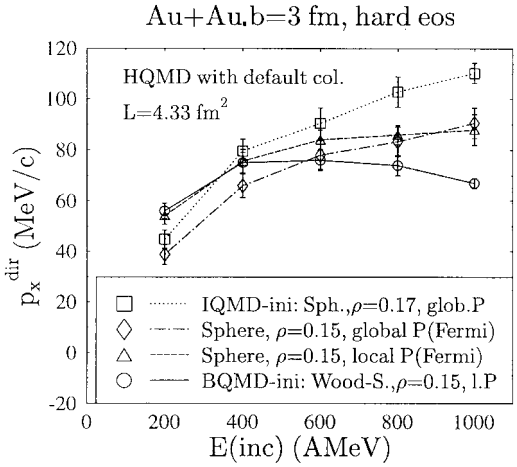

Fig. 5. Excitation function of the system Au+Au at $b = 3$ fm impact parameter obtained with HQMD (default collision term) using the BQMD initialisation, a hard sphere initialisation with reduced Fermi momentum and with full Fermi momentum and the IQMD initialisation

initial state versus vibration modes. For the IQMD initialisation the maximum stability is reached for $L = 8.66\,\mathrm{fm}^2$ at about $\rho = 0.17\mathrm{fm}^{-3}$ and at about $\rho = 0.15\mathrm{fm}^{-3}$ for $L = 4.33\,\mathrm{fm}^2$.

The differences in the flow results between BQMD and IQMD motivated to search for parameters which might influence the flow. There are three major differences between BQMD and IQMD calculations: Besides the interaction range they concern the initialisation, the cross-sections employed and the different values for the saturation density. For a better comparison we changed in the following the interaction range of IQMD to $L = 4.33\,\mathrm{fm}^2$. As a first step we investigate the dependence on the initialisation of the nuclei, which also includes the role of the value of ρ_0. The BQMD and IQMD initialisations differ in three aspects: a) the shape of the coordinate distribution of the particles, b) the average central density in the nucleus and c) the limitation of the Fermi momentum to the value obtained by a local density approximation or the full Fermi momentum, respectively.

The dependence on each of these differences is studied in Fig. 5 which shows results of a HQMD calculation with inclusion of modules from BQMD and IQMD. It demonstrates that the very same dynamics, i.e. same forces, same cross-sections and same equations of motion lead to considerably varying results depending on the initial conditions chosen.

Here IQMD-ini (squares) denotes the default IQMD initialisation with $L = 4.33\,\mathrm{fm}^2$. using hard sphere for the centroids, no constraint to the Fermi-momentum and $\rho_{ini} = \rho_0 = 0.17\,\mathrm{fm}^{-3}$. The diamonds describe a calculation with a different initial density $\rho_{ini} = 0.15\,\mathrm{fm}^{-3}$. We see a reduction of the flow at highest densities. This effect is known from hydrodynamical studies using the Rankine-Hugoniot equations. [84]. It should be noted that the values obtained with $L = 4.33$ obtained at $\rho_{ini} = 0.15\,\mathrm{fm}^{-3}$ (i.e. at maximum stability) are comparable with the values obtained with $L = 8.66\,\mathrm{fm}^2$ and $\rho_{ini} = 0.17\,\mathrm{fm}^{-3}$ i.e. at maximum stability for the $L = 8.66\,\mathrm{fm}^2$ case.

The triangles denote a calculation where additionally the Fermi momenta are constrained by the binding energy (similar as done in BQMD). Here we see an enhancement of the flow at low energies. Besides the flat shape of the excitation function this constraint on the Fermi momentum also causes strong fluctuations of the rms radii [8]. As a consequence – as we will see later – this introduces a considerable systematic error of the flow values.

BQMD-ini (circles) finally denotes the BQMD default with a Wood Saxon distribution, the local constraints of the Fermi momentum and the saturation density of $\rho_{ini} = 0.15\,\mathrm{fm}^{-3}$. Since the density profile is now smeared out even more an additional reduction of the flow can be found at high energies.

The composition of all three effects causes the BQMD-initialisation to yield a very flat excitation curve while for the IQMD-initialisation a strong dependence of the flow on the incident energy is observed.

It should be noted that similar effects as reported for the flow are also found for the particle production. These effects are weaker but lead to the same picture. Effects that simulate a weaker repulsion and thus cause a weaker flow will yield an enhanced particle production.

The collision term also influences the excitation function of flow. It was found that the collision terms of IQMD and HQMD yielded about the same values while the BQMD collision term causes a decrease of about 5-10 MeV/c relativ to the IQMD collision term.

The different p_x^{dir} values reflect themselves in different dependences of p_x on the rapidity. Figure 6 compares the transverse momentum in the reaction plane $p_x(y)$ for the system Au(1AGeV)+Au at b=3 fm impact parameter. We see that IQMD gives values similar to VUU while BQMD yields much lower flow values close to beam and target rapidity. It should furthermore be noted that similar effects have been found in the analysis of the flow out of plane.

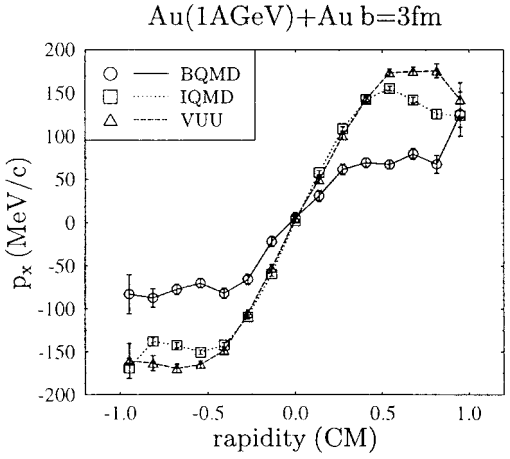

Fig. 6. Comparison of the transverse flow $p_x(y)$ of nucleons in the reaction Au(1 AGeV)+Au b=3 fm for VUU, IQMD and BQMD, all using a hard equation of state without momentum dependent interactions

BQMD yields a less pronounced squeeze-out as compared to VUU and IQMD.

In conclusion it is found that the description of the flow depends strongly on the detailed description of the initial state of the nuclei as well as on the interaction range. The constraints on the Fermi momentum as used in BQMD lower the Fermi pressure and yield a nearly flat excitation function of the flow which is in contradiction to current data.

3 Fragment production

Another key issue for heavy ion reactions is the simultaneous production of several intermediate mass fragments, i.e. clusters which are heavier than α's but considerably lighter than typical fission products. This phenomenon, usually referred to as multifragmentation, has lead to numerous speculation that this may be the signal for the occurrence of a liquid vapor transition in nuclear matter [85].

A lot of studies involving QMD models addressed this issue as well. QMD does not explicitly include a phase transition, even more so, it is a non-equilibrium transport theory, where equilibrium need not necessarily be established to be applicable to multifragmentation reactions, as it is the case in statistical models for nuclear fragmentation [86].

It should be noted that there exist problems in describing the properties of Fermi systems at low temperature [46,87]. However, it should also be noted that the fragment distributions obtained with QMD are in the range of the different statistical models [53]. The difference between the distributions from QMD and these models is in the same order the differences between those models themselves.

QMD predicted the emission of several fragments in a single event, qualitatively similar to the experimental observations and at lower energies also quantitatively [51, 25,26,52].

A realistic description of fragmentation processes within QMD is one of the most complicated tasks. At higher bombarding energies ($E > 400$ MeV/nucleon) fragment formation is already a rather rare process. At lower energies, where multifragmentation is a major reaction channel (between 50 and 200 MeV/nucleon), the reaction is slowed down, which requires a improved accuracy of the calculation.

One aspect is that single nuclei at rest also start to evaporate nucleons and fragments after 50–100 fm/c. This effect has to be minimized which sets stringent conditions on the stability of single nuclei. Moreover the nuclear binding needs to be properly described.

At 50 MeV/nucleon beam energy for a symmetric system, each nucleon carries 12.5 MeV kinetic energy in the center of mass. Together with a binding energy of about 8 MeV per nucleon, only 4.5 MeV/nucleon are available in the center of mass. This has severe implications on the required accuracy of the description of ground state nuclei. If the binding energy is missed by only 1 MeV/nucleon, then a 22% different total energy is used in the calculation. At 100 MeV/nucleon this uncertainty still amounts to 6%.

One crucial aspect, as far as the fragmentation properties of QMD are concerned, is the interaction range which is directly related to the width of the gaussian wavepackets. More extended wave packets i.e. a long interaction range leads to a smaller number of fragments. These fragments are somewhat heavier than those fragments from simulations with smaller wavepackets. This behavior has essentially two reasons: in the case of broader gaussians, particles in a cluster are bound to a larger number of other nucleons inside the cluster. On the other hand, with a smaller width the fluctuations are enhanced and an excited nucleus dissolves more easily.

For example, BQMD with a Gaussian width of $L = 4.33$ fm^2 gives 12.7 IMFs in Au (150 MeV/nucleon) + Au at b=3 fm. IQMD with more extended gaussians ($L = 8.66\, fm^2$) yields 6.6 IMFs only. It should be noted that in the present analysis the charge has not been regarded (especially since BQMD has no explicit charges). Therefore we used $5 \leq A \leq 19$ for the numbers obtained above. However, if we employ the same Gaussian width for both models we obtain almost the same results. This can be seen in Fig. 7 where the fragment mass spectra have been compared for both models using both interaction ranges.

Parameters other than the interaction range, e.g. the value of the saturation density or the different treatment of Fermi momenta do not affect the intermediate mass fragment multiplicity significantly. We also find no differences on the different cross sections or potentials.

The range of Yukawa forces do not significantly influence the mass distribution of the fragments as it was found for the Au(150AMeV)+Au at $b = 3$ fm. This observable shows only dependence on the Gaussian width.

In conclusion it can be stated that the interaction range shows strong significance on the fragment produc-

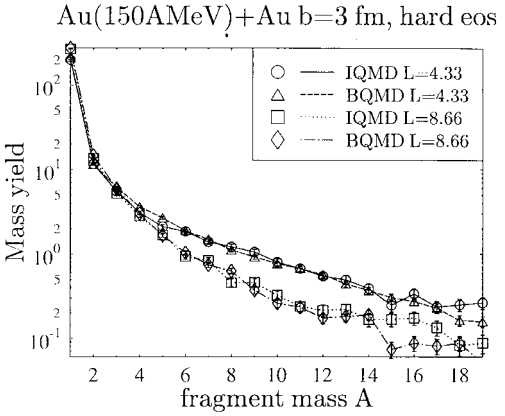

Fig. 7. Fragment mass distribution obtained by BQMD and IQMD for the system Au(150 MeV) + Au b=3 fm, both with $L = 4.33\,\mathrm{fm}^2$ and $L = 8.66\,\mathrm{fm}^2$

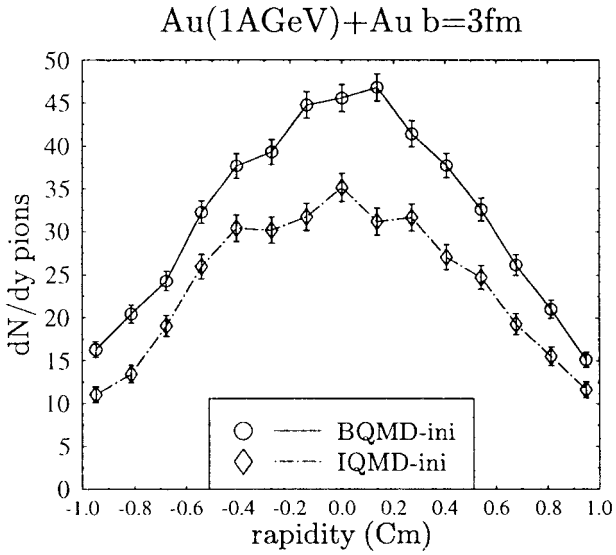

Fig. 8. Rapidity distributions of pions for Au(1 GeV/nucleon)+Au reactions at b=3fm obtained with QMD employing the BQMD initialisation (circles) and the IQMD initialisation (diamonds)

tion. The smaller values of $L = 4.33\,\mathrm{fm}^2$ used in BQMD show much better agreement to existing data as $L = 8.66\,\mathrm{fm}^2$ used in IQMD. Furthermore BQMD shows a better stability against particle evaporation and better binding energies. This is due to the constraints on the Fermi momentum as well as to the Yukawa potentials. The vibration modes resulting from the Fermi momentum constraints do not show strong influences on the fragmentation, at least in central collisions. Although the initialisation does not have a strong influence on the fragmentation pattern in central collisions, an initialisation which combines both, a proper binding energy (as it is achieved in BQMD) and a proper density profile (as it is done in IQMD) is preferred. This achievement is one of the main design goals of a new molecular dynamics scheme of the QMD type [89].

4 Particle production

Let us now turn to the question of particle production. In the regarded energy domain mainly the production of pions and subthreshold kaons is of interest.

Concerning the description of pion production the results of BQMD are not regarded, since it has no free pions and the cross section parametrization was not adapted to pion physics. Instead we will compare HQMD and IQMD. It is found that the cross section parametrizations of HQMD and IQMD yield very similar results. The change of the interaction range changes the pion multiplicity by only 5–10%. A strong influence can, however, be obtained from the initialisation procedure. As an example, rapidity distribution of pions are displayed in Fig. 8. The two calculations differ only in the initialisation, forces and cross-sections are identical in both cases. The BQMD initialisation (that with the lower density) yields about the same shape of the pion rapidity distribution as a calculation using the IQMD initialisation. The absolute number of produced pions is about 30-40% larger in the case of the BQMD initialisation.

The difference cannot be explained neither by Pauli blocking nor by absorption effects. It is found that although the calculation with the IQMD-initialisation yields higher densities, the calculation with a BQMD-initialisation shows higher collision numbers. This corresponds to the fact that up to maximum compression calculations with a BQMD-initialisation loose compressional energy (and thus gain kinetic energy) while calculations with an IQMD-initialisation gain compressional energy and loose kinetic energy.

The arguments used in the discussion of the flow (see Fig. 5) still hold for the particle production. The different parts of the initialisation which cause an increase of the flow yield correspondingly a decrease of the pion number. For Au(1 AGeV) +Au $b = 3$ fm the change of the initialisation density from 0.17 to $0.15\,\mathrm{fm}^{-3}$ yields (for $L = 4.33\,\mathrm{fm}^2$) an increase of about 20 % and the change from a hard sphere initialisation to a Woods-Saxon type initialisation another enhancement of about 15 %. The constraints on the Fermi momentum yield no visible influences on the pion number at 1 AGeV energies.

It should furthermore be stressed that all regarded models (VUU, IQMD, HQMD) perform a delta decay using a lifetime which is the inverse of the mass-dependent decay-width. Changes concerning this description might have strong effects on the rapidity distributions.

The study of subthreshold kaon production is motivated by the strong dependence of the kaon multiplicity on the nuclear eos [41,73,80,82]. It has been found that a hard equation of state yields a stronger repulsion and lower densities of the compression region than a soft eos [88]. Therefore a hard eos shows stronger flow and a smaller kaon multiplicity. The pion multiplicity shows only slight dependences on the eos since both equations of state yield about the same compression densities [4,88].

Kaon production have not been studied within the BQMD model but with an upgrade version called QMDRKNC [80]. This version does not include free pions, therefore the deltas have an infinite lifetime. A first comparison of this version with IQMD has been presented in [73]. The kaon numbers obtained with both models agree for Au (1 AGeV) +Au within 20-30%. HQMD with $L = 4.33\text{fm}^2$ and BQMD initialisation yields about the same values. HQMD differs mainly from QMDRKNC in the lifetime of the deltas. The similar multiplicities of IQMD and QMDRKNC are a result of counterbalancing effects which will be briefly discussed:

The infinite lifetime of the delta in BQMD and QMDRKNC causes an enhancement of about 10 - 20% of the kaon number when compared to HQMD. This is due to the dominance of the channel nucleon+delta → nucleon+hyperon+kaon for the subthreshold production. An infinite lifetime enhances the possibilities for nucleon-delta collisions. Similar numbers have been found when comparing default IQMD with an calculation with infinite delta lifetimes.

The BQMD initialisation yields an enhancement of the kaon production by about 20 - 30 % as compared to the IQMD initialisation. The reason is presumingly similar to that for the pion production. The BQMD initialisation allows higher kinetic energies of the nucleons in the compressed state.

The choice of a short Gaussian width ($L = 4.33\,\text{fm}^2$, BQMD default) causes a reduction of the kaon number of about 30 % as compared to a calculation with $L = 8.66\,\text{fm}^2$ which is the IQMD default for Au. The reason for this may be connected to the argument used for explaining the enhancement of flow when using a short width. The density gradient gets steeper when the interaction range decreases. This simulates a stronger repulsion of the compressed nuclear matter.

5 Initialisation and Stability

One of the seminal problems of the simulation of a heavy ion reaction is the proper description of ground state nuclei. One cannot expect that a reaction is reproduced properly if projectile and target do not have the observed properties, in particular the proper ground state density.

As we have stressed several times before the choice of the initial condition is crucial for a proper description of various phenomena. Fermi-momenta treated semiclassically as a random motion of nucleons inside a nucleus induces significant fluctuations of the density profile, if the motion of a single nucleus is followed for some time.

Figure 9 shows a time evolution of the root mean square radii of single Au nuclei in coordinate and momentum space. Concerning the coordinate space we observe an expansion mode in IQMD and an oscillation mode in BQMD. IQMD shows best stability if potentials corresponding to a hard eos is used whereas BQMD shows best stability if a soft eos is used. The rms radii obtained with BQMD soft eos correspond to the results presented in [8]. The other eos yield larger fluctuations for both programs.

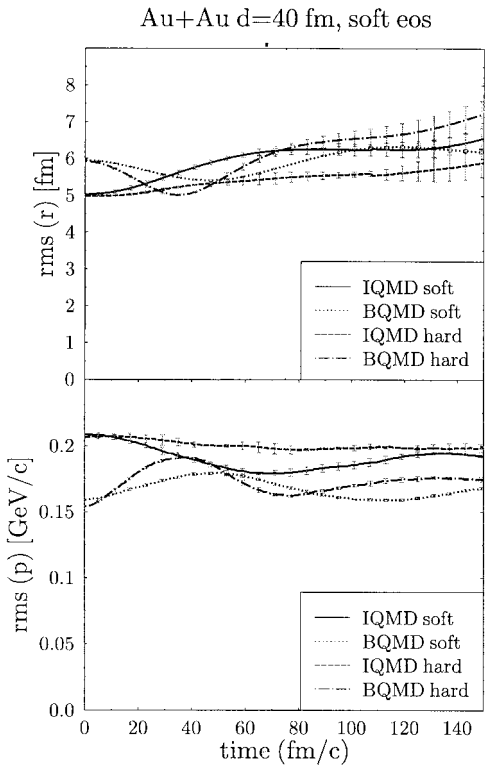

Fig. 9. Time evolution of the root mean square radii of a single Au nucleus in coordinate and momentum space obtained with IQMD and BQMD using a hard and a soft eos

This stresses once more the fact that a semiclassical approach can be optimized to a desired purpose but on the cost of other applications.

The fluctuations of the rms radii in momentum space demonstrate that the potentials are not saturated in the given initialisation. The system converts potential energy into kinetic energy and vice versa to equilibrate the system. This conversion of energy was already addressed in the previous subsection (particle production). The initialisations of IQMD and BQMD yield different pion numbers due to different balances of kinetic and potential energy.

The counterbalancing parts are the kinetic pressure which causes an expansion and the density dependence of the potentials which may cause attraction for low densities and repulsion for high densities.

For this it may be interesting to regard the mean density of the system which is the mean value of the density of each particle averaged over all particles. It should be noted that this value may be sensible to density fluctuations in the center which do only slightly effect the root mean square radius.

A time evolution of single nuclei the Au case (hard eos) mean densities (density per particle averaged over all particles) changing between about $\rho = 0.14$ and 0.15 fm^{-3} for IQMD and between $\rho = 0.11$ and 0.18 fm^{-3} for BQMD. For smaller systems (on a time period of about 60 fm/c) the stability of IQMD gets smaller, to e.g. a range of $\rho = 0.14$ to 0.17 fm^{-3} for a Nb nucleus in IQMD, $\rho = 0.16$ to 0.19 fm^{-3} for a Ca nucleus in IQMD and $\rho = 0.16$ to

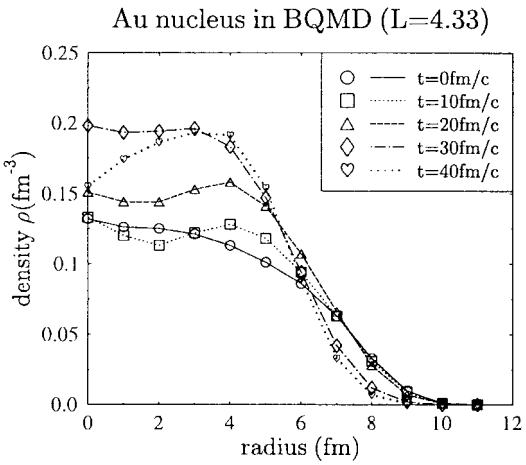

Fig. 10. Time evolution of the density profiles $\rho(r)$ obtained for a Au nucleus initialized with BQMD (with Yukawa) using the width of $L = 4.33\,\mathrm{fm}^2$

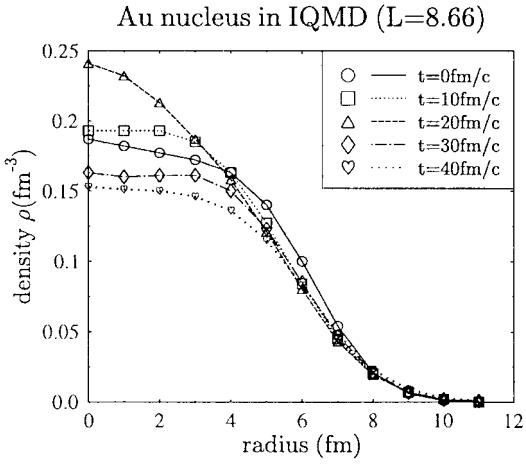

Fig. 11. Time evolution of the density profiles $\rho(r)$ obtained for a Au nucleus initialized with IQMD using the width of $L = 8.66\,\mathrm{fm}^2$

$0.21\ \mathrm{fm}^{-3}$ for a Ne nucleus in IQMD, while in BQMD the fluctuations remain constant ($\rho = 0.1 - 0.17\,\mathrm{fm}^{-3}$) for all three regarded systems. It should also be noted that these fluctuations increase in IQMD if a soft eos is used (about $\rho = 0.11 - 0.15$ for the Au case) and decrease in BQMD (to about the same values).

Let us now examine the density profile of a single Au nucleus. Figure 10 displays the time evolution of the density profile within BQMD. We observe a change in the center as well as at the surface. In a considerably large volume around the center ($r \leq 5$ fm) the change of density with time induces changes of the compressional energy in a heavy ion reaction. The weakening of the surface causes an increase of the rms radius and it therefore modifies the total interaction cross section as well as the probability of e.g. particle production processes in particular in peripheral collisions. Without Yukawa forces these fluctuations are even larger. The reason for these fluctuations are the lack of pressure built up by the Fermi momentum when the nucleus gets compressed. This can be verified by initializing HQMD with the full Fermi momentum but otherwise as above.

The time evolution of the density profile in IQMD is displayed in Fig. 11 for a gold nucleus with the default width of $L = 8.66\,\mathrm{fm}^2$. We find strong fluctuations at $r = 0$ but a stable shape at the surface and a rather stable rms radius. We also find that the shape of the $r^2\rho(r)$ distribution shows better stability for the $L = 8.66\,\mathrm{fm}^2$ case than for $L = 4.33\,\mathrm{fm}^2$. This also motivated the choice of L in IQMD.

It has now to be tested whether these fluctuations of the density profile cause uncertainties in the determination of observables. This is tested by changing the initialisation distance d (with respect to the minimum distance for a head-on collision) which is defined as (R are the radii of the nuclei):

$$d = z(\text{center of proj.}) - z(\text{center of target}) - R(\text{proj.}) - R(\text{targ.})$$

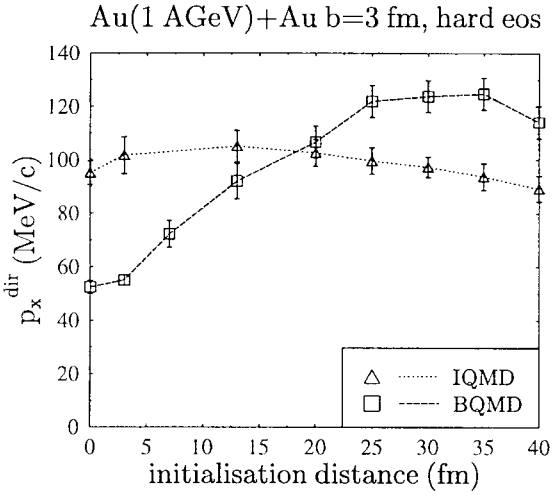

Fig. 12. Dependence of the flow obtained from the system Au(1 AGeV)+Au at b=3fm on the initialisation distance using IQMD with $L = 8.66\,\mathrm{fm}^2$ and BQMD with $L = 4.33\,\mathrm{fm}^2$

By changing this distance we allow the nuclei to change their profile according to the internal forces before they come into nuclear contact. For the ideal case this technical parameter should have no influence on the observables. In reality the observables depend on it, however, in most cases weakly.

A strong influence of the density fluctuations on observables has been found particularly within BQMD for the collective sideward flow. Depending on the initially chosen distance the total directed transverse momentum transfer in the reaction Au (1 GeV/nucleon, $b = 3\,\mathrm{fm}$) + Au varies strongly as it can be seen in fig,12. Although the absolute magnitude of the flow depends on whether a Yukawa interaction is employed or not, this variance is observed in both cases. IQMD, however, run with the default parameters shows a much weaker dependence on this technical parameter. In the calculation the flow varies as a function on the initialisation distance only by about

Table 4. Comparison of the different realizations BQMD, HQMD and IQMD concerning the different ingredients of the inputs

Input	BQMD	IQMD	HQMD
Initialisation	Wood-Saxon	hard sphere	both
Init. distance	3fm	0fm	3fm
Gaussian width	4.33 fm^2	8.66 fm^2	4.33 fm^2
Coulomb forces	$Z_p = Z_n$	$Z_p = 1, Z_n = 0$	$Z_p = Z_n$
Yukawa forces	L=1.5 fm	L=0.4 fm	none
Yukawa adjust.	$t_1(i) = t_1 - \sum_j U_{ij}^{Yuk}/\rho$	$t_1 = t_1 - \kappa * V_0^{Yuk} * L^{Yuk}/L^{3/2}$	none
actio = reactio	on the average	'exact'	'exact'
asymmetrie forces	none	$t_6/\rho_0\, T_3^i T_3^j\, \delta(\boldsymbol{r}_i - \boldsymbol{r}_j)$	none
forces on π	no π	Coulomb	no force
cross sections	Cugnon 1981	VUU 1986	Cugnon 1989
particles	N, Δ	N, Δ, π	N, Δ, N^*, π

10%. An IQMD calculation with $L = 4.33\,\mathrm{fm}^2$ shows less stability. The flow values are decreasing with initialisation distance. This corresponds to the effect that the density of maximum stability ($\rho = 0.15\,\mathrm{fm}^{-3}$ for $L = 4.33\,fm^2$) is not equal to the initialisation density $\rho_{ini} = 0.17\,\mathrm{fm}^{-3}$. This was originally the motivation for the use of a system dependent width in IQMD. A BQMD calculation with $L = 8.66$, however, still shows strong fluctuations. The fluctuations in BQMD decrease if the Fermi momentum of the initialized nuclei is increased. However, in this case the binding energy of the nucleus becomes smaller and spurious particle evaporation may be effected.

For the observables for Au(1GeV)+Au discussed in this paper we find the following maximum deviation (in a range of initialisation distances between 0 and $d_{max} =$ 13 fm) from the default values: for the IQMD initialisation 10% concerning flow and kaon multiplicity and 8% concerning pion multiplicity and for the BQMD initialisation 70% concerning flow, 45% concerning kaon and 35% concerning pion multiplicity. For the fragmentation of Au(150Mev)+Au b=3fm both models yield (in their default modes) about 8-15% deviation in the number of IMFs (a rise from 6.6 to about 7.1 for IQMD and a fall from 12.7 to about 10.8 for BQMD).

It should be noted that the reported errors also include about 5-10% statistical fluctuations and that for initialisation distances larger than 13 fm the deviations may still increase for some calculations. The value of 13 fm has been chosen since it is the difference in the effective distance to the first reaction point between a central and a very peripheral collisions.

In any case, these fluctuations cause an additional systematic error which has to be added to the statistical one if one compares with data. Because these fluctuations are stronger using a BQMD initialisation the systematical error is larger there.

In conclusion we find that both models show fluctuations of the density profile at $r = 0$. However IQMD shows in its default mode a rather stable $r^2\rho(r)$ shape while for BQMD the maximum of $r^2\rho(r)$ changes in time. This yield artificial vibration modes which influence the stability of the nucleus and therefore cause systematic errors which in most cases are stronger in BQMD than in IQMD. Especially the discussion of dynamical variables like flow and particle production within BQMD has to be regarded very cautiously.

V Summary and concluding remarks

We have compared different realizations of the Quantum Molecular Dynamics model. The different realizations differ in certain input variables as they are comparatively presented in Table 4. Some of these parameters are purely technical, some are physical. The latter parameters are constrained by experimental observations but are not completely fixed. If the same parameters are employed the result of the different programs are identical in between the error. This is a remarkable achievement in view of the several thousand program lines of each of these programs.

The HQMD realization allows for the first time to compare in detail the influence of different inputs on the different observables. The most important input is the choice of the Gaussian width L or in other words the interaction range of the nuclear potential. A change of the interaction range causes differences in the density profile of a ground state nucleus and in the strength of the density gradient. Thus a smaller interaction range yields an enhanced flow, enhanced fragment production and (which was not shown) a reduced numbers of pions (slight changes) and kaons (larger changes). The interaction range determines the surface properties of the nuclei as well as their binding energy. Only in infinite nuclear matter the binding energy is independent of this quantity. The experimental value of these observables allow to fix the range of possible values.

The choice of the cross section employed in HQMD, BQMD or IQMD yield slight changes in the flow (and also slight differences in the stopping) but has no influences on the fragmentation. Pion production in HQMD and IQMD are comparable.

An important factor is the choice of the ground state description. This choice effects the results in flow and particle production, but does not influence the fragmentation pattern. The flow at high energies is found to be stronger if the initialisation of the nucleus is more compact. At low energies these differences vanish, instead the average

Fermi momentum becomes important. The Fermi momentum corresponding to (infinite) nuclear matter are necessary to stabilize the nucleus against artificial vibrations and yield better agreement with experimental flow data. At the same time a large Fermi momentum lowers the binding energy. The binding energy of heavy nuclei is reproduced if local Fermi momenta are employed.

As a conclusion we find that there are variables which are very robust against a change of the technical or physical parameters, e.g. the rapidity distribution. Others like the fragmentation pattern depend on the range of the interaction only. Other observables, like the directed flow have a very strong dependence on many details of the calculation and slight differences between the different QMD flavours yield large differences in this observable.

In the BQMD proper binding energies have been achieved on the cost of large dynamical fluctuations in the initial state and by a moderate energy non-conservation ($\approx$ 2 MeV/nucleon for single nuclei) on an event by event basis. The IQMD-model offers rather stable density distributions and good energy conservation, however for the price of nucleon evaporation and and improper binding energies ($E_{bind} \approx 4-5$ MeV/nucleon for heavy nuclei instead of 8 MeV/nucleon).

The choice between a parametrization which yields the proper ground state energy of projectile and target and that which yield the necessary Fermi momentum to obtain the observed flow is not satisfying. Therefore work is in progress to modify the bare interaction between the nucleons inside the nucleus in a way which allows to obtain both at the same time. In particular one has to account for the peculiar dependencies between the various parts of the model. Initialisation, propagation, hard collisions, and Pauli-blocking cannot be treated independently from each other. Forces and cross-sections are connected. The specific choice of the saturation density, and thus also that of the central density of heavy nuclei influences the physical output. These aspects are part of the effort to obtain a new unified QMD scheme which covers the energy range between 25 MeV/nucleon and 200 GeV/nucleon. The aim of this new model will be to cover the best possibilities for a reliable description of the different aspects of heavy ion collisions [89].

This work was in part supported by the French Institut National de Physique Nucléaire et de Physique des Particules (IN2P3), by the German Bundesministerium für Bildung und Forschung (BMBF), by the Deutsche Forschungsgemeinschaft (DFG) and by the Gesellschaft für Schwerionenforschung (GSI).

References

1. W. Scheid, R. Ligensa, and W. Greiner. Phys. Rev. Lett. **21**, 1479 (1968)
2. L. P. Csernai and J. I. Kapusta. Phys. Reports **131**, 225 (1986)
3. R. Stock. Phys. Reports **135**, 261 (1986)
4. H. Stöcker and W. Greiner. Phys. Reports **137**, 277 (1986)
5. R. B. Clare and D. Strottman. Phys. Reports **141**, 179 (1986)
6. B. Schürmann, W. Zwermann and R. Malfliet. Phys. Reports **147**, 3 (1986)
7. W. Cassing, V. Metag, U. Mosel and K. Niita. Phys. Reports **188**, 361 (1990)
8. J. Aichelin. Phys. Reports **202**, 233 (1991)
9. H. Stöcker, J. A. Maruhn and W. Greiner, Phys. Rev Lett. **44**, 725 (1980)
10. H. Stöcker, L. P. Csernai, G. Graebner, G. Buchwald, H. Kruse, R. Y. Cusson, J. A. Maruhn and W. Greiner, Phys. Rev **C25**, 1873 (1982)
11. H. Stöcker, W. Greiner, and W. Scheid. Z. Phys. **A286**, 121 (1978)
12. P. Danielewicz. Nucl. Phys. **A314**, 465 (1979)
13. H. Stöcker, A. A. Ogloblin and W. Greiner. Z. Phys. **A303**, 259 (1981)
14. S.A. Bludman, Phys. Reports 163 (1988) 47
15. H.A. Gustafsson et al., Phys. Rev. Lett. 52 (1984) 1592; D. Beauvis et al., Phys. Rev. C27 (1983) 2443; H.G. Ritter et al., Nucl. Phys. A447 (1985) 3c; K.G.R. Doss et al., Phys. Rev. Lett. 57 (1986) 302; H.H. Gutbrod et al., Phys. Lett. 216B (1989) 267.;H.H. Gutbrod et al. Rep. Prog. Phys. 52 (1989) 1267
16. A. Sandoval et al., Phys. Rev. Lett. **45**, 1236 (1980); R. Stock et al., Phys. Rev. Lett. **49**, 1236 (1982); J. Harris et al., Phys. Lett. **B153**, 377 (1985)
17. H. Kruse, B. V. Jacak, and H. Stöcker. Phys. Rev. Lett. **54**, 289 (1985)
18. G.F. Bertsch, H. Kruse and S. Das Gupta. Phys. Rev. **C29**, R673 (1984)
19. J. Aichelin and G. Bertsch. Phys. Rev. **C31**, 1730 (1985)
20. C. Gregoire, B. Remaud, F. Sebille, L. Vinet, and Y. Raffray, Nucl. Phys. **A465**, 317 (1987)
21. H. Feldmeier. Nucl. Phys. **A515**, 147 (1990)
22. A. Ono, H. Horiuchi, T. Maruyama and A. Ohnishi. Phys. Rev. Lett. **68**, 2898 (1992)
23. J. Aichelin and H. Stöcker. Phys. Lett. **B176**, 14 (1986)
24. Compare eg. [8,51] with T. Wienold et al, submitted to Phys. Rev. Lett. or [49,77,81]
25. P.B. Gossiaux, D. Keane, S. Wang, and J. Aichelin, Phys. Rev. C **51**, 3357 (1995)
26. P.B. Gossiaux, and J. Aichelin, Phys. Rev. C -submitted
27. J. J Molitoris and H. Stöcker, Phys. Rev **C32**, R346 (1985)
28. E. A. Uehling and G. E. Uhlenbeck. Phys. Rev. **43**, 552 (1933) and Phys. Rev. **44**, 917 (1934)
29. E. Suraud, S. Ayik, M. Belkacem, J. Stryjewski, Nucl. Phys. A542 (1992) 141
30. Y. Yariv and Z. Frankel. Phys. Rev. **C20**, 2227 (1979)
31. J. Cugnon. Phys. Rev. **C22**, 1885 (1980)
32. G. Peilert, H. Stöcker, A. Rosenhauer, A. Bohnet, J. Aichelin and W. Greiner. Phys. Rev. **C39**, 1402 (1989)
33. A.R. Bodmer and C.N. Panos. Phys. Rev. **C15**, 1342 (1977)
34. L. Wilets, Y. Yariv and R. Chestnut. Nucl. Phys. **A301**, 359 (1978)
35. S.M. Kiselew and Y.E. Pokrovskil. Sov. Journ. Nucl. Phys. **38**, 46 (1983)
36. J.J. Molitoris, J.B. Hoffer, H. Kruse and H. Stöcker. Phys. Rev. Lett. **53**, 899 (1984)
37. A.K. Kermann and S.E.Koonin, Ann. Phys. 100 (1976) 332

38. L. G. Arnold et al. Phys. Rev. **C25**, 936 (1982)
39. G. Passatore. Nucl. Phys. **A95**, 694 (1967)
40. G. F. Bertsch and S. Das Gupta, Phys. Rep. **160**, 189 (1988)
41. J. Aichelin, A. Rosenhauer, G. Peilert, H. Stöcker, and W. Greiner. Phys. Rev. Lett. **58**, 1926 (1987)
42. S. Hama et al. Phys. Rev. **C41**, 2737 (1990)
43. Ch. Hartnack and J. Aichelin Phys. Rev. **C49**, 2801 (1994)
44. W. Botermanns and R. Malfliedt, Phys. Lett. **B 215**, 617 (1988) and Phys. Rep. **198**, 115 (1990)
45. W. Cassing and U. Mosel, Prog. Nucl. Part, Phys.**25**, 1 (1990)
46. G. Peilert, J. Konopka, M. Blann, M. G. Mustafa, H. Stöcker and W. Greiner. Phys. Rev. **C46**, 1457 (1992)
47. J. Cugnon, T. Mizutani and J. Vandermeulen. Nucl. Phys. **A352**, 505 (1981)
48. T. Kodama et al, Phys. Rev. C29 (1984) 2146
49. Ch. Hartnack. PhD thesis, GSI-Report 93-5 (1993)
50. J. Aichelin, C. Hartnack, A. Bohnet, Li Zhuxia, G. Peilert, H. Stöcker and W. Greiner. Phys. Lett. **B 224**, 34 (1989)
51. A. Bohnet et al. Phys. Rev. **C44**, 2111 (1991)
52. M. Begemann-Blaich et al. Phys. Rev. **C 48**, 610 (1993)
53. W.F.J. Müller et al. Phys. Lett. **B 298**, 27 (1993)
54. S.C. Jeong et al. Phys. Rev. Lett. 72, 3468 (1994)
55. P.B. Gossiaux et al. Phys. Rev. **C 51**, 3357 (1995)
56. S. Huber and J. Aichelin. Nucl. Phys. **A573**, 587 (1994)
57. J. Cugnon, private communication
58. C. Hartnack, L. Zhuxia, L. Neise, G. Peilert, A. Rosenhauer, H. Sorge, J. Aichelin, H. Stöcker, and W. Greiner. Nucl. Phys. **A495**, 303 (1989)
59. B. J. VerWest and R. A. Arndt. Phys. Rev. **C25**, 1979 (1982)
60. Ch. Hartnack, H. Stöcker, and W. Greiner. In H. Feldmeier, editor, *Proc. of the International Workshop on Gross Properties of Nuclei and Nuclear Excitation, XVI, Hirschegg, Kleinwalsertal, Austria* (1988)
61. S. A. Bass, C. Hartnack, H. Stöcker and W. Greiner. Phys. Rev. Lett. **71**, 1144 (1993)
62. S. A. Bass, C. Hartnack, H. Stöcker and W. Greiner. Phys. Rev. **C 51** , 3343 (1994)
63. Ch. Hartnack, J. Aichelin, H. Stöcker and W. Greiner. Mod. Phys. Lett. **A9**, 1151 (1994)
64. Ch. Hartnack, J. Aichelin, H. Stöcker and W. Greiner. Phys. Lett. **B 336**, 131 (1994)
65. S. Soff et al. Phys. Rev. **C 51**, 3320 (1995)
66. R. Madey, W.M. Zhang et al. Phys. Rev. **C 42**, 1068 (1990)
67. G. Claesson et al. Phys. Lett. **B 251**, 23 (1990)
68. V. Ramilien et al. Nucl. Phys. **A 587**, 802 (1995)
69. C. Dorso, S. Duarte, and J. Randrup, Phys. Lett. B **188**, 287 (1987)
70. G. Peilert, J. Randrup, H. Stöcker, and W. Greiner, Phys. Lett. B **260**, 271 (1991)
71. J. Konopka, H. Stöcker, and W. Greiner, Nucl. Phys. **A583**, 357c (1995)
72. J. Jaenicke, J. Aichelin, N. Ohtsuka, R. Linden, A. Faessler, Nucl. Phys. **A536**, 201 (1992)
73. C. Hartnack, J. Jaenicke, L. Sehn, H. Stöcker, J. Aichelin, Nucl. Phys. **A 580**, 643 (1994)
74. H. Sorge, H. Stöcker, W. Greiner, Ann. Phys. 192, 266 (1989)
75. E. Lehmann, R.K. Puri, A. Faessler, G. Batko, S.W. Huang. Phys. Rev. **c 51**, 2113 (1995)
76. R.K. Puri, E. Lehmann, A. Faessler, S.W. Huang. Zeitsch. f. Physik **A 351**, 59 (1995)
77. Ch. Hartnack, S.A. Bass, J. Aichelin, H. Stöcker and W. Greiner, In J. Aichelin and D. Ardouin, editors, *Int. Workshop on Multiparticle Correlations and Nuclear Reactions (Corinne II), Nantes*, World Scientific, Singapore (1994)
78. Ch. Hartnack et al. Nucl. Phys. **A 538**, 53 (1992)
79. Ch. Hartnack, J. Aichelin, H. Stöcker and W. Greiner, Phys. Rev. Lett. 72, 3767 (1994)
80. J. Aichelin and J. Jaenicke, Proc. Workshop on Meson production, interaction and decay, Cracow (Poland), may 1991, ed. A. Magiera, World Scientific (Singapore) 1992
81. Ch. Hartnack, J. Aichelin, H. Stöcker, W. Greiner, Proc. of the 7th Intern. Conf. on Nucl. Reaction Mechanisms, Varenna (Italy), June 1994, ed. E. Gadioli, Ricerca Scientifica ed Educazione Permanente, Univ. di Milano (Italy), p.242
82. A. Lang et al. Nucl. Phys. A541, 507 (1992)
83. J. Randrup and C.M. Ko, Nucl. Phys. A 343, 519 (1980).
84. H. Stöcker, private communication
85. J. Pochodzalla et al. Phys. Rev. Lett. 75 (1995) 1048
86. A.S. Botvina et al., Nucl. Phys. A 584 (1995) 737
87. R. Donangelo and S.R. Souza, Phys. Rev.C 52 (1995) 326
88. Ch. Hartnack, H. Stöcker and W. Greiner, Proc. of the NATO Advanced Study Institute on the Nuclear Equation of State, Peniscola (Spain), 1989, ed. H. Stöcker and W. Greiner, Plenum, New York, NASI series B216 A, p. 239
89. S.A. Bass et al., Proc. on the Int. Conference on modern physics at the turn of the millenium, Wilderness (South Africa), World Scientific, ed. A. Gallmann and H. Stöcker. L. Winckelmann et al., Contribution to the proceedings of the International Conference on Quark Matter 1996, Heidelberg (Germany).